remote sensing

MDPI

Article

On the Use of Sentinel-2 NDVI Time Series and Google Earth Engine to Detect Land-Use/Land-Cover Changes in Fire-Affected Areas

Rosa Lasaponara [1], Nicodemo Abate [2,*], Carmen Fattore [1], Angelo Aromando [1], Gianfranco Cardettini [1] and Marco Di Fonzo [3]

[1] Institute of Methodologies for Environmental Analysis (CNR—IMAA), National Research Council, C.da S. Loja, 85050 Tito Scalo, Italy
[2] Institute of Heritage Science (CNR—ISPC), National Research Council, C.da S. Loja, 85050 Tito Scalo, Italy
[3] Comando Carabinieri per la Tutela Forestale, Via Carducci No. 5, 00187 Roma, Italy
* Correspondence: nicodemo.abate@ispc.cnr.it

Abstract: This study aims to assess the potential of Sentinel-2 NDVI time series and Google Earth Engine to detect small land-use/land-cover changes (at the pixel level) in fire-disturbed environs. To capture both slow and fast changes, the investigations focused on the analysis of trends in NDVI time series, selected because they are extensively used for the assessment of post-fire dynamics mainly linked to the monitoring of vegetation recovery and fire resilience. The area considered for this study is the central–southern part of the Italian peninsula, in particular the regions of (i) Campania, (ii) Basilicata, (iii) Calabria, (iv) Toscana, (v) Umbria, and (vi) Lazio. For each fire considered, the study covered the period from the year after the event to the present. The multi-temporal analysis was performed using two main data processing steps (i) linear regression to extract NDVI trends and enhance changes over time and (ii) random forest classification to capture and categorize the various changes. The analysis allowed us to identify changes occurred in the selected case study areas and to understand and evaluate the trend indicators that mark a change in land use/land cover. In particular, different types of changes were identified: (i) woodland felling, (ii) remaking of paths and roads, and (ii) transition from wooded area to cultivated field. The reliability of the changes identified was assessed and confirmed by the high multi-temporal resolution offered by Google Earth. Results of this comparison highlighted that the overall accuracy of the classification was higher than 0.86.

Keywords: wildfire; land-use/land-cover change; Sentinel-2; random forest; linear regression; machine learning; Google Earth Engine

Citation: Lasaponara, R.; Abate, N.; Fattore, C.; Aromando, A.; Cardettini, G.; Di Fonzo, M. On the Use of Sentinel-2 NDVI Time Series and Google Earth Engine to Detect Land-Use/Land-Cover Changes in Fire-Affected Areas. *Remote Sens.* **2022**, *14*, 4723. https://doi.org/10.3390/rs14194723

Academic Editors: Wu Xiao, Qiusheng Wu and Xuecao Li

Received: 4 August 2022
Accepted: 16 September 2022
Published: 21 September 2022

1. Introduction

Wildfires are considered one of the most significant causes of environmental disturbance and damage, capable of affecting the functionality of ecosystems and generating complex socio-economic impacts at local and global levels. The phenomenon of wildfires is extremely complex as it depends on several aspects, including those related to the characteristics of vegetation, morphology, meteorological conditions, and, above all, anthropic factors.

The use of satellite data makes supports the monitoring and management of forest fire before, during, and after the emergency and at different spatial/temporal scales (from global down to a local scale). In particular, the ability to monitor post-fire dynamics and detect post-fire changes is crucial to understanding forests' response to wildfire (especially under changing climate conditions) and the anthropogenic impact on the fragile fire-affected areas.

In recent decades, the problem of forest fires has profoundly increased in intensity and frequency, due to anthropogenic and natural phenomena, including climate change,

the abandonment of rural areas, and the constant loss of biodiversity that makes agro-forestry systems increasingly fragile. Hence, land-use/land-cover changes in fire-affected areas are generally not allowed and in some cases, as in Italy, prohibited by law in order to discourage arsonists and facilitate the post-fire vegetation recovery (see, for example, Italian law n. 353/2000). Preserving the "natural capital" and adopting good practices to monitor and support the sustainability of ecosystem goods and services is a priority today. In this context, satellite can provide a valuable support for setting up reliable and effective monitoring systems. In particular, satellite data can provide synoptic information systematically updated and, with modern facilities, also available free of charge. For these reasons, the use of satellite technologies for the monitoring of forest resources can, in some aspects, be considered a consolidated practice although, obviously, the ever-increasing availability of information and data and the latest technological developments have opened up new frontiers and applications.

Today, the availability of big and open data, such as datasets available from NASA (MODIS, Landsat satellites [1–6] etc.) and ESA (Sentinels [7–16]), and the developments in information and communication technologies (ICT), including cloud-based resources, have supported the massive increase of the use of satellite for change detection and analysis, based on various methods and techniques [13,17–26] including artificial intelligence (AI) and, therefore, machine learning (ML) and deep learning (DL) [11,27–36].

Land-use/cover-change (LUCC) analyses can be divided into two macro-category techniques based on: (i) comparison of two or multiple dates and (ii) time-series analyses.

(i) Techniques focused on comparing two (or multiple) dates comparison can be split into approaches based on a post-classification comparison (PCC) and procedures based on a direct comparison, generally known as comparative pre-classification [37–41].
(ii) Multi-temporal analysis methods can be split into: (i) temporal segmentation algorithms, such as CCDC (continuous change detection and classification), VERDeT (vegetation regeneration and disturbance estimates through time), and LandTrend [41–48]; and (ii) trend analysis [49–56] to detect land-use/land-cover changes by analyzing the pixel-in-time signal [47,57–60].

Compared to the techniques based on comparing two (or multiple) dates, the time series methods are generally more complex and time consuming due to the amount of data, but they are expected to be suitable for the identification of both slow and fast changes such as, for example, those due to parasites, salinization, deforestation, or wildfires. Both of these methods, coupled with socio-economic parameters [61–63], can be a useful basis for the definition of metrics and indicators of SDGs (Agenda 2030).

In recent years, one of the main issues has been the ability to store and work with big data. To date, there have been many solutions proposed to overcome this problem and to take advantage of open and big datasets made available for free or for a fee. One of these systems, probably one of the most widely used, is Google Earth Engine [64,65], an open-source tool [66–68] that provides various datasets and tools [18,25,27–29,51,65,69,70,70–82]. The strength of a cloud-based computing system, which includes ready-to-use and up-to-date datasets, is the ability to use computing power without having to download large amounts of data locally.

Several initiatives have been developed using Google Earth Engine (GEE), such as (i) Global Forest Watch [80,81] and (ii) Global Surface Water [83], useful for the monitoring of forests and water, respectively. More recently, GEE has also been used for the analysis of natural events with high impact on the landscape, such as wildfires, landslides, and floods [18,26,70,73,74,84–86].

The purpose of this work is to evaluate the potential offered by the combined use of high spatial and temporal resolution satellite data (such as Sentinel-2) and cloud computing systems (such as Google Earth Engine) to capture land-use and land-cover changes occurred in fire-affected areas. This poses challenges, since the aim is the identification of small changes (at the pixel level) in disturbed environs, because they are already affected by fire, which generally occurs over large areas of at least several hectares.

To capture both slow and fast changes, the investigations focused on NDVI time series, selected because they are expected to be suitable for the purpose of our investigations, being extensively used for both the monitoring of vegetation's post-fire behaviours, as in [87–92], and the assessment of changes in vegetation cover [47,57–60].

For each fire considered, the study covered the period from the year after the event to the present. The multi-temporal analysis was performed using two main data processing steps (i) linear regression to extract NDVI trends and enhance changes over time and (ii) random forest classification to capture and categorize the various changes.

2. Materials and Methods

2.1. Study Area

This study was carried out to identify land-use/land-cover changes in fire-affected sites located in several regions of the Italian peninsula (shown in Figure 1). In Italy, according to Italian law (n. 353/2000), an area is subject to restrictions for ten years after a fire. These restrictions prohibit anyone from changing the land use without a permit from the Italian Ministry of the Environment and Land and Sea Protection (Ministero dell'Ambiente e della Tutela del Territorio e del Mare).

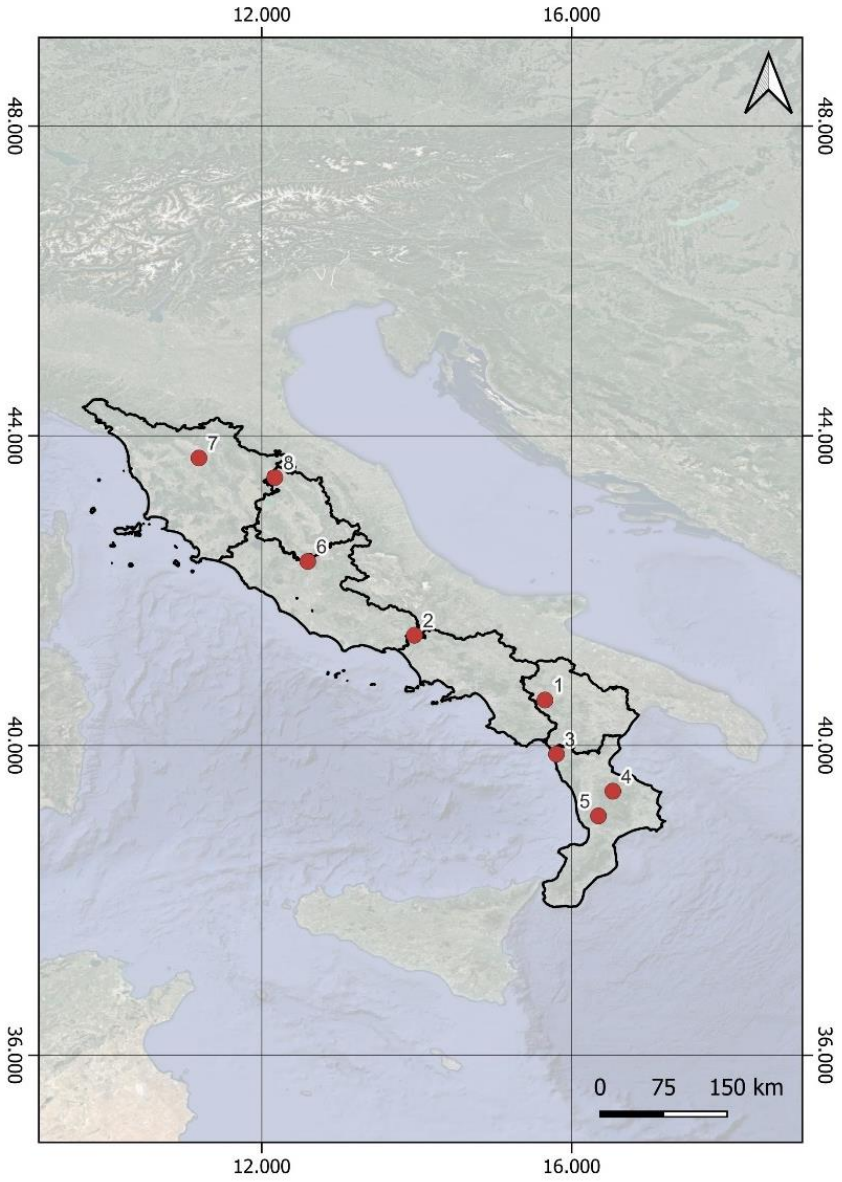

Figure 1. Areas of interest refer to the IDs in Table 1.

Table 1. Summary table of wildfire events considered as case studies.

Region	Year	Area (ha) Approx.	ID
Basilicata	2015	13,176	1
Campania	2015	9180	2
Calabria	2017	33,249	3
Calabria	2017	43,692	4
Calabria	2012	39,495	5
Lazio	2017	6104	6
Toscana	2016	5284	7
Umbria	2017	8464	8

The area considered for this study is the central–southern part of the Italian peninsula, in particular the regions of (i) Campania, (ii) Basilicata, (iii) Calabria, (iv) Toscana, (v) Umbria, and (vi) Lazio (Figure 1). For the purpose our study, NDVI time series have been investigated because they are considered a reliable tool to assess post-fire vegetation recovery dynamics, and therefore it is expected that it will be suitable for identifying land-use/land-cover changes in fire-affected sites.

2.2. Methodological Approach Rationale, Tools, and Datasets

The rationale of the approach we adopted is based on the consideration that methods for the identification of changes in long time series of vegetation indices, such as NDVI, must enable the characterization/classification of different types of changes and trends from the seasonal components of time series. Changes occurring in the seasonal component indicate phenological changes, whereas changes occurring in the trend component often indicate disturbances such as those linked to climate change or specific events such as fires, floods, or extreme meteorological conditions (drought, wind), or those induced by parasite/insect attacks. Methodological approaches for extracting useful and meaningful information from time series must be capable of detecting the subtle changes/trends within the time series (heavily influenced by fire occurrence) which can be completely veiled or hidden by seasonal variations. Moreover, the subtle changes/trends to be identified are generally partially or totally unknown and characterized by very subtle spectral variations in fire-affected areas. The ability and effectiveness of change detection approaches and methods depends on the ability to account for the great variability exhibited by seasonal variations (at seasonal and/or intra-annual scales) while identifying small multi-year trends and changes at diverse inter-annual timescales.

Therefore, today there are still numerous open issues and scientific challenges. In particular, among the great variety of unanswered questions, the following ones seem to require particular attention:

(i) What type of data processing can be adopted to suitably transform spectral information into vegetation parameters?
(ii) What is the minimum mapping unit (pixel, cadastral parcel, or segment level) to be considered from satellite Sentinel-2?

In order to contribute towards answering these questions, Sentinel-2 NDVI time series data were processed following the workflow shown in Figure 2. NDVI time series have been already successfully used by a group of authors to characterize the vegetation dynamic and behavior after fire, and to identify a proxy indicator of vegetation fire resilience, as per [87–91]. NDVI is the most widely used index for vegetation health status analyses [92,93]. It is widely used to identify the health of vegetation and provides information on the spatial and temporal distribution of vegetation communities and biomass. High values of the vegetation index identify pixels covered by substantial proportions of healthy vegetation [94]. Therefore, variations in NDVI values and in general in vegetation indices are indicative of variations in ongoing vegetation trends and dynamics. Vegetation's dynamical processes are difficult to study since they affect the complex soil–surface–atmosphere system, due to the existence of feedback mechanisms involving human activity, ecological patterns, and various subsys-

tems of climate. The use of satellite time series along with statistical analysis techniques can be helpful in understanding the functional characteristics of vegetation dynamics and enable the reporting of ongoing trends at a detailed level [24,38,87,88,95,96].

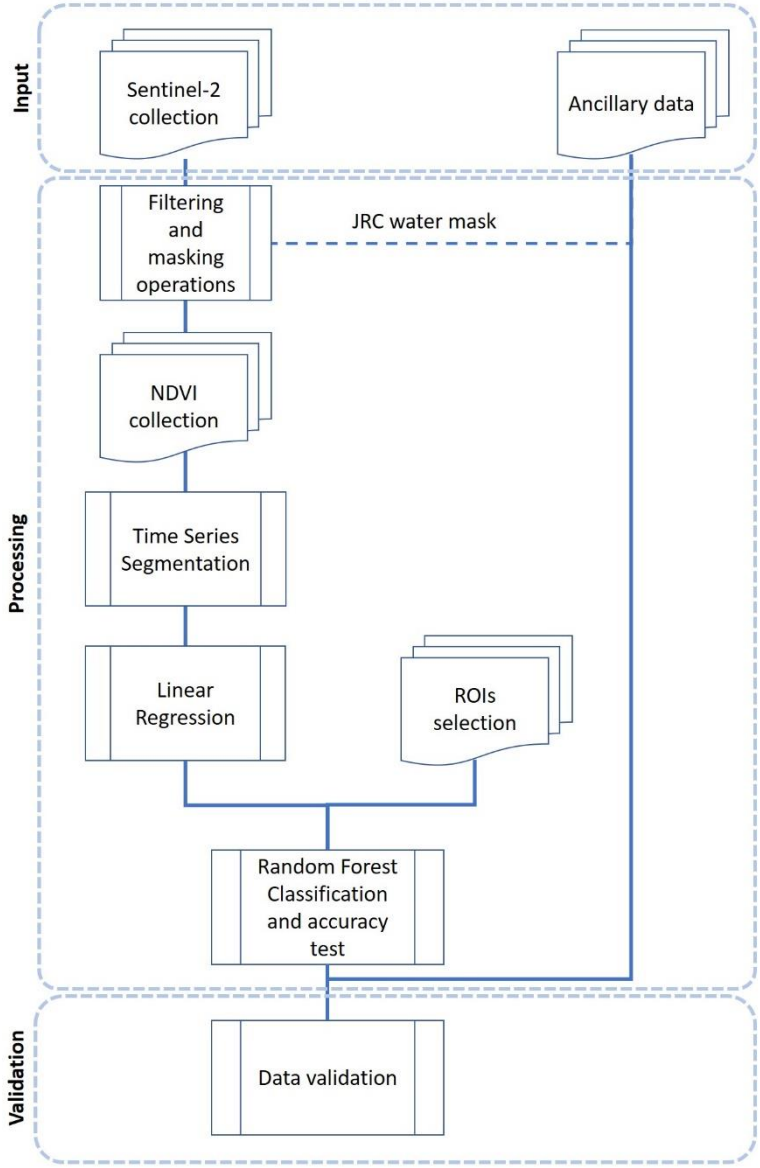

Figure 2. Flowchart.

For the purpose of our investigations, Sentinel-2 data were chosen for their spatial (10 m/pixel), spectral, and temporal (revisit time five days) resolution. Sentinel-2 BOA (Bottom Of the Atmosphere) data [7] were processed using GEE tools along with ancillary data used to (i) identify areas of interest, previously affected by fire and (ii) improve the classification and interpretation.

The areas of interest were selected using shapefiles provided directly by the Carabinieri Corps, relating to wildfires that occurred in the regions of Campania, Basilicata, Calabria, Toscana, Lazio, and Umbria between the years 2012 and 2017 (Table 1).

The ancillary data used were: (i) CORINE land cover (CLC) provided by the Copernicus Programme, for the years 2012 and 2018, at 100 m/pixel [97–99], to get an overview of land cover in areas of interest; (ii) NASA SRTM Digital Elevation at 30 m [100] and its derivatives [101,102] (elevation and slope) to get an overview of the morphology of the

area of interest; (iii) Google Earth high-resolution images to obtain a visual validation of the change; and (iv) JRC Global Surface Water Mask to mask the water out [83].

2.3. Methods

The whole data processing chain (see flowchart in Figure 2) is subdivided into three blocks, divided into operations of (i) input, (ii) processes, and (iii) validation.

The method, devised to identify land-use/land-cover changes that have occurred in fire-affected areas, is based on two main steps, (i) the linear regression (LR) LUCC method to quickly and easily obtain the information needed to understand any changes over time and (ii) random forest classification to categorize the various dynamics of change that have occurred in the land use/land cover.

The whole procedure started from the shape of the burnt areas (provided by the Carabinieri). For each shape, all the images in the Sentinel-2 dataset were processed if characterized by a cloudiness of less than 20% and acquired in the year after the fire occurrence. In addition, facilities available from GEE were used to mask (i) clouds, (ii) cloud shadows, (iii) snow, and (iv) water [103], as suggested in the documentation provided by the developers (https://developers.google.com/earth-engine/tutorials/community/sentinel-2-s2cloudless, accessed on 3 August 2022) and described in [104]. Filtering and masking operations were applied to the entire collection considered, using an image-by-image calculation.

NDVI maps were computed using the appropriate GEE function, "normalizedDifference (['B8', 'B4'])", where B8 and B4 are the near infrared and red bands of the Sentinel-2 sensor, respectively. Once this operation was completed, the system proceeded to separate the entire collection on a temporal basis, according to a given time window. The time window considered for these analyses was year by year, and the annual collection was created based on the average values of the NDVI index.

The linear regression (LR) LUCC method was chosen because it is useful for detrending data and reducing stationarity along a time series, thus enabling us to (i) obtain the information needed to understand any changes over time and (ii) easily classify and/or threshold the data.

This type of analysis is particularly useful for understanding events that occurred at a specific location or in a restricted area, and for separating "extraordinary" events that affected a pixel from ordinary events related to seasons and weather conditions. The analysis started by calculating and adding dependent variables (e.g., vegetation indices) and independent variables (e.g., time), over the entire time series considered at the pixel level over time [60,96,105]:

$$x_t = \beta_0 + \beta_1 z_{t1} + \beta_2 z_{t2} + \cdots + \beta_q z_{tq} + w_t \quad (1)$$

where x_t is the linear regression model, $\beta_0 + \beta_1 z_{t1} + \beta_2 z_{t2} + \cdots + \beta_q z_{tq}$ are unknown fixed regression coefficients, and w_t is a random error or noise.

For each pixel, the output provided two parameters called "slope" and "offset" [45,96]. Both slope and offset products were merged into a single stack to be classified using a ML (random forest classifier) to identity and categorize the pixels characterized by (i) no significant changes, (ii) negative changes, and (iii) positive changes in the NDVI trends.

The accuracy of the classification was assessed using the regions of interest (ROIs) and by comparison with independent datasets made up of high-resolution images available in GEE (the code is fully described by GEE developers at https://developers.google.com/earth-engine/apidocs/ee-classifier-smilerandomforest, accessed on 3 August 2022).

For each change type (see Section 3), the training points (ROIs) were selected and randomly split to have the 60% points as training and the 40% as testing to compute the kappa and accuracy [106–109].

To determine the best-performing number of trees to be used in the RF, the hyperparameter tuning method (described in [104] for each case study) was used (Figure 3).

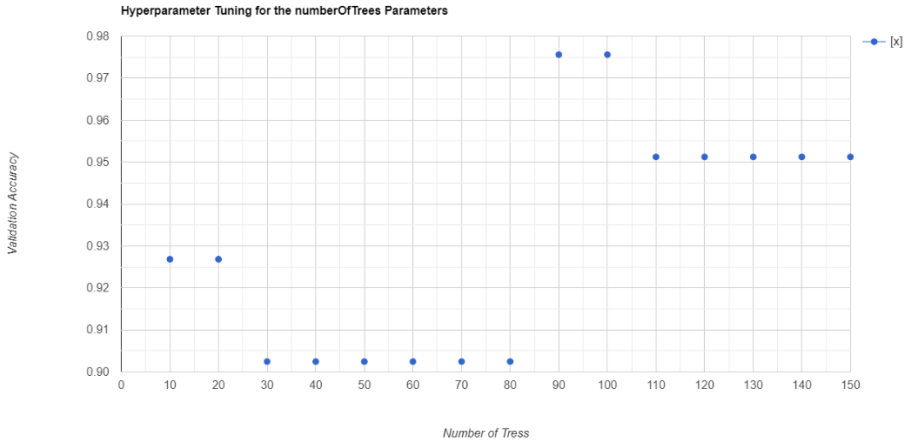

Figure 3. Example of hyperparameter tuning of random forest classification applied to case study ID 5 (Table 1).

3. Results and Discussion

The use in Google Earth Engine of LR and ML applied to the annual average value of the NDVI provided interesting results for all the analyzed case studies. In particular, offset and slope/scale were suitable in the identification of the areas of change and highlighted them both (i) quantitatively, in numerical terms, and (ii) visually in chromatic terms, through the RGB and in the use of the single-band display as well. The RGB composition (obtained from R: slope, G: offset, B: slope) showed the change zones with (i) blue (or close to blue), (ii) green (or close to green), and (iii) yellow (or close to yellow) tones (Figure 4).

The analysis of the values of the selected ROIs showed common values between the analyzed events, with the same trend of offset and slope in the three classes identified as (i) type-1 change, (ii) type-2 change, and (iii) no change (Figure 5a). A similar signal was observed for the slope alone, which showed negative and positive values in areas with higher change and values very close to zero in the areas with a stable signal over time (Figure 5b). The identification of areas where the LULC (Land Use Land Cover) has changed over time in the post-fire period was also significantly distinguishable from the value that the slope/scale pixels assume. In fact, from the ROIs identified, type-1 change is characterized by a positive offset and a slope always greater than 0; type-2 change, on the contrary, presents a positive offset but a slope always less than 0; and stable signal areas have a positive offset but the slope oscillates with values very close to ± 0 (Figures 5c, 6 and 7).

Moreover, the results from the RF classifications (obtained as described in Section 2.3) provided excellent and accurate results (Table 2), with less blurry images and well-defined groups of pixels (Figure 8).

LR provided good results as a method to identify changes in time series. In more detail, the following various types of land-use/land-cover change were identified in the analyzed case studies: (i) woodland felling, (ii) remaking of paths and roads, and (ii) transition from wooded area to cultivated field. All of these changes were confirmed by the high multi-temporal resolution offered by Google Earth (Figures 9 and 10).

Table 2. Test accuracy and kappa: summary table of wildfire events considered as case studies.

ID (Referring to IDs in Table 1)	Test Accuracy	Test Kappa
1	0.88	0.82
2	0.92	0.89
3	0.92	0.83
4	0.89	0.84
5	0.91	0.86
6	0.9	0.84
7	0.95	0.90
8	0.86	0.79

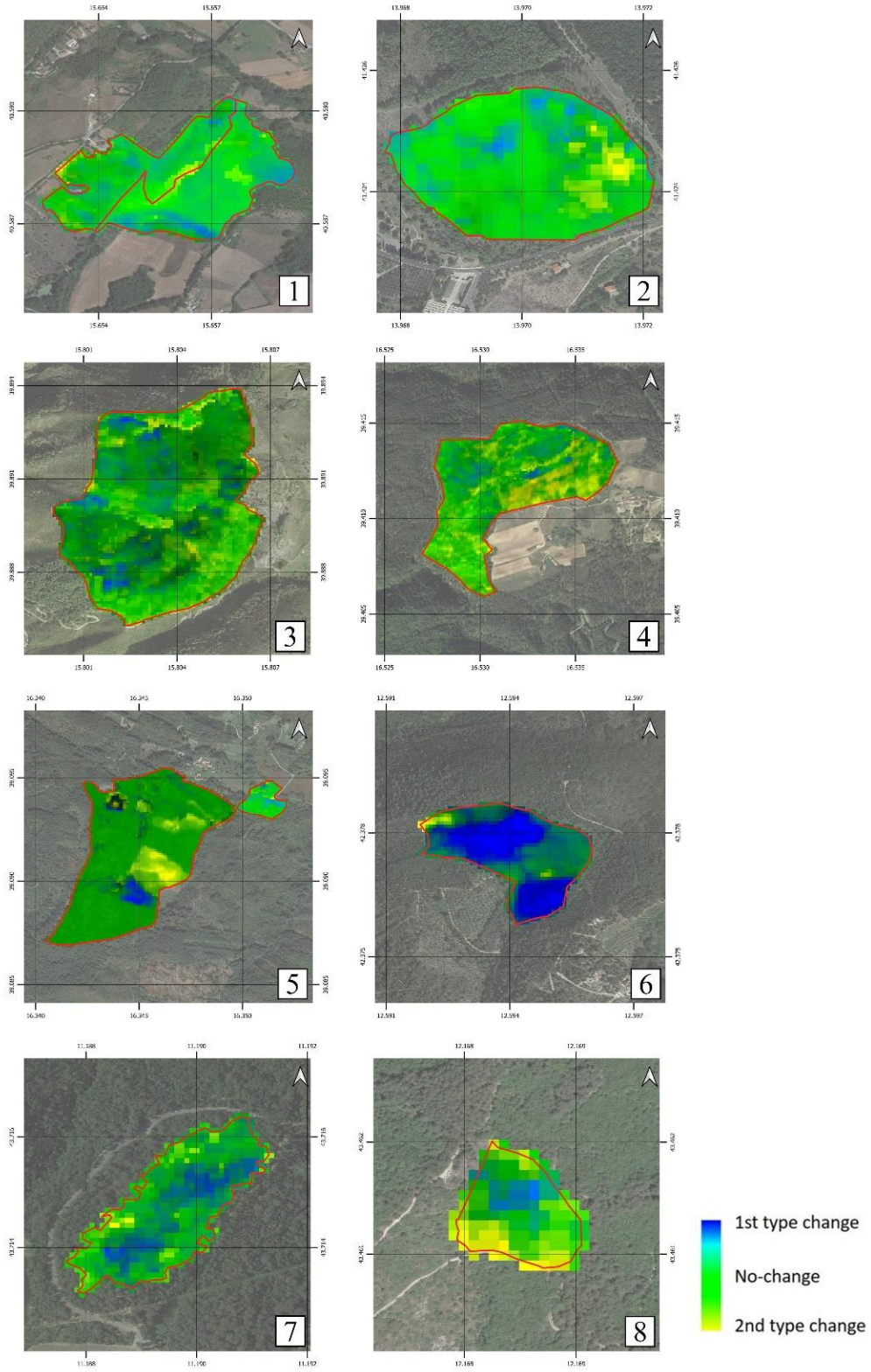

Figure 4. RGB of the results of the analysis applied to the fire-affected areas. The numbers correspond to the IDs shown in Table 1.

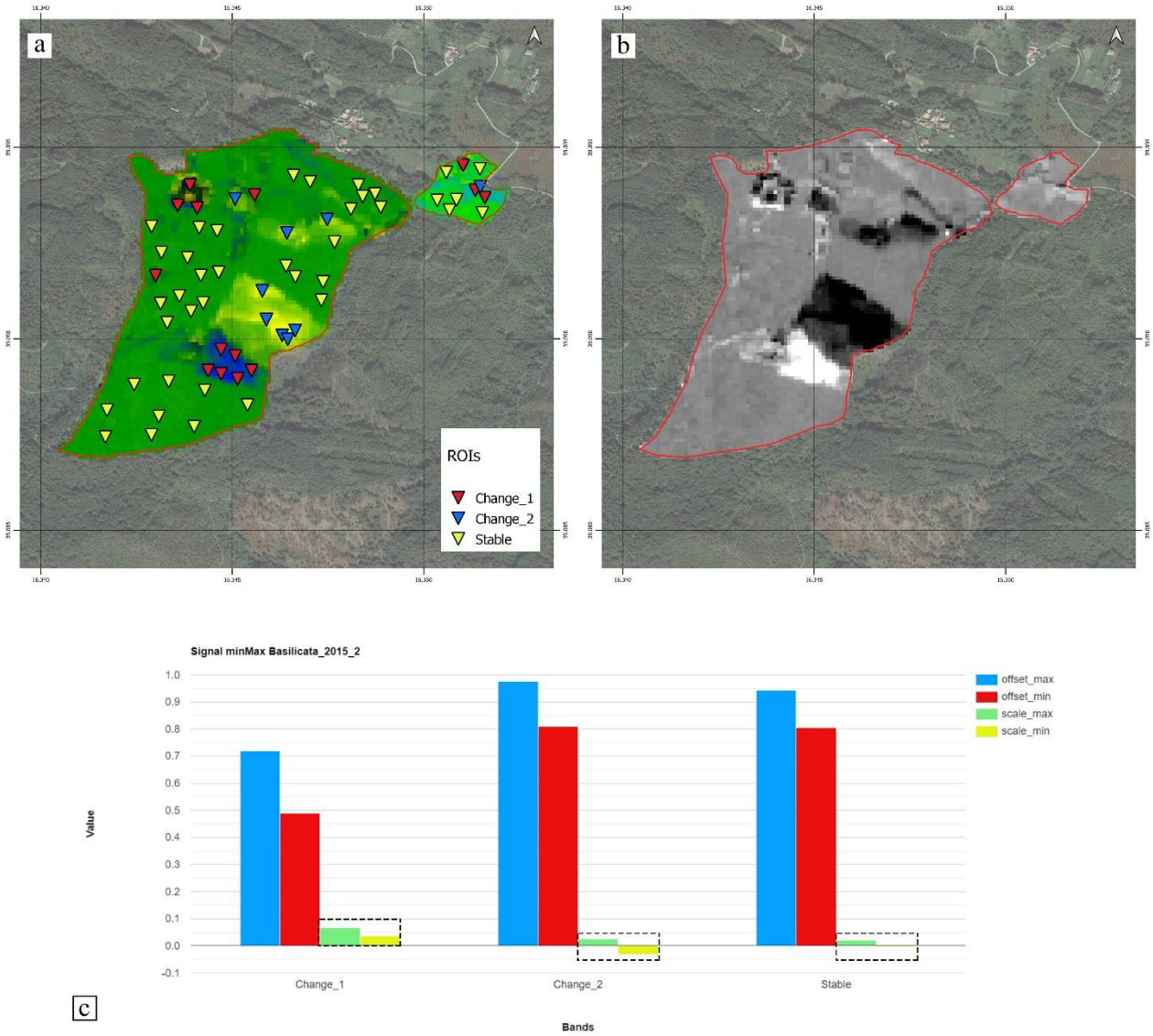

Figure 5. (**a**) RGB obtained using R: slope, G: Offset, B: slope; (**b**) single-band image of slope (scales): positive values are light, negative values are dark, grey areas represent values very close to 0; (**c**) pixel value graph obtained from ROIs in (**a**).

The analysis of the results showed that the RGB images obtained by using R: slope (min: 0, max: minimum value of the slope), G: offset (min: 0, max: maximum value of the offset), and B: slope (min: 0, max: maximum value of the slope) assumed constant and comparable behavior between the analyzed case studies (Figure 6).

At the same time, this signal was still analyzable using only slope values as a single-band image, as shown in Figure 5b. The analysis of the individual signals extracted from the selected pixel value via ROIs also showed a very good consistency in signal behavior between cases (Figures 6 and 7).

The identified signals point towards three types of trends in pixel value and behavior over time:

First type: tending to blue in RGB images and white in single-band greyscale images: positive slope (upward trend), which is due to growth (NDVI value) over time of the analyzed signal. The offset values assumed by these pixels were on average lower than those assumed in the pixels of the other two types of observed behavior.

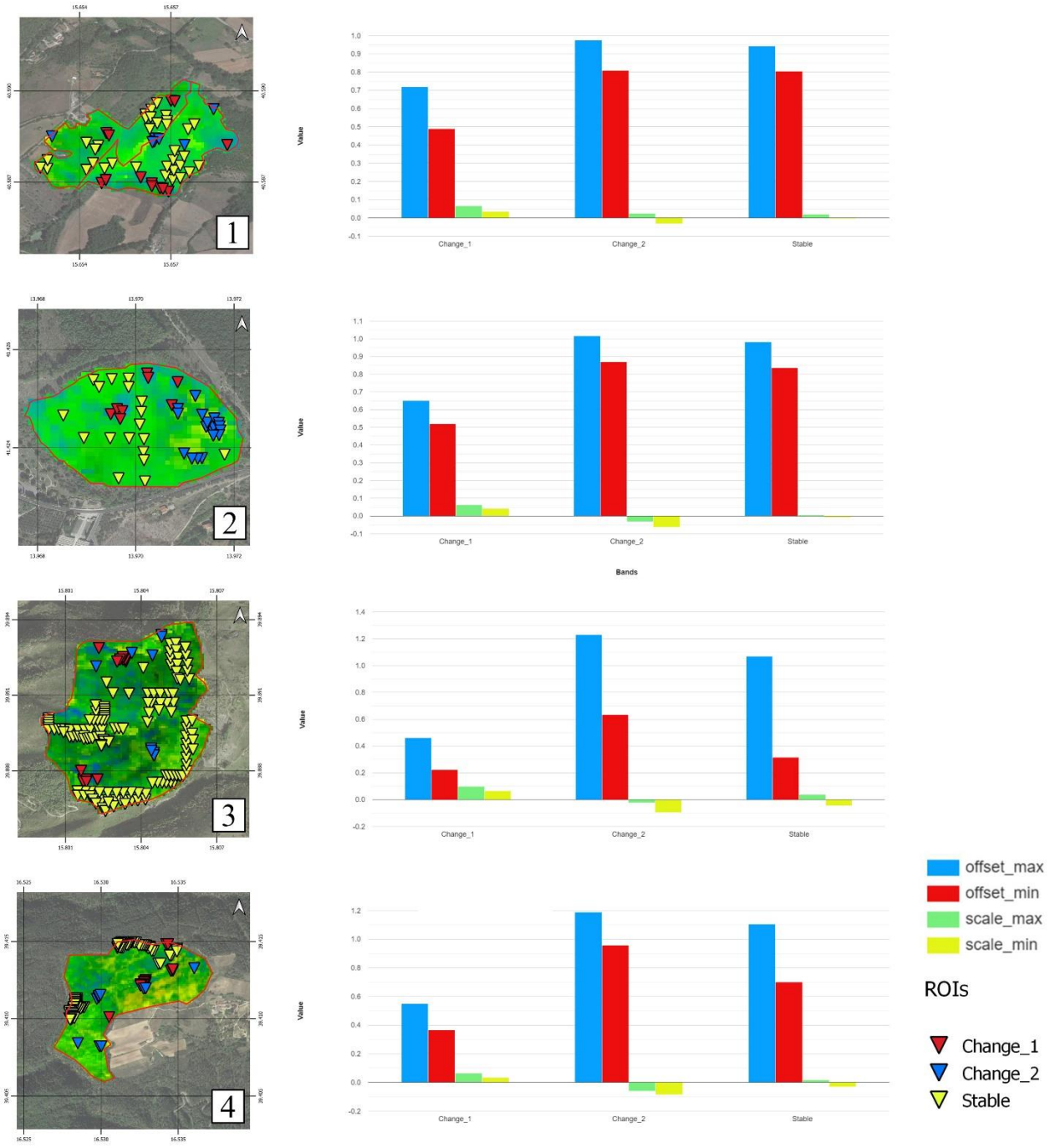

Figure 6. Events 1–4 (referring to IDs in Table 1). Overview image of analyzed cases (RGB: slope, offset, slope) and graph of pixel value in selected ROIs.

Second type: tends to yellow in RGB images and black in single-band greyscale images: negative slope (negative trend), due to the decrease in the signal (NDVI value) analyzed over time. The offset values assumed by these pixels were on average higher than those assumed in the pixels of the other two types of behavior observed.

Third type: tends to green in RGB images and grey in single-band greyscale images: stable signal over time (stable trend) without changes in the LULC. The offset values assumed by these pixels were on average higher than those assumed in the pixels of the first type, and lower than those assumed in the pixels of the second type. On the other hand, the slope assumes values very close to ± 0.

From a spectral and spatial point of view, the recognition of events that had occurred appeared to be quite reliable, as demonstrated in Figures 9 and 10. This methodology also allowed us to highlight very small changes, compatible with the spatial resolution of Sentinel-2 data.

Similarly, the classification provided a much more defined clustered picture than trends alone (Figure 8). However, the accuracy of the classification was high enough to justify its use and to prefer it over trend images alone (Table 2).

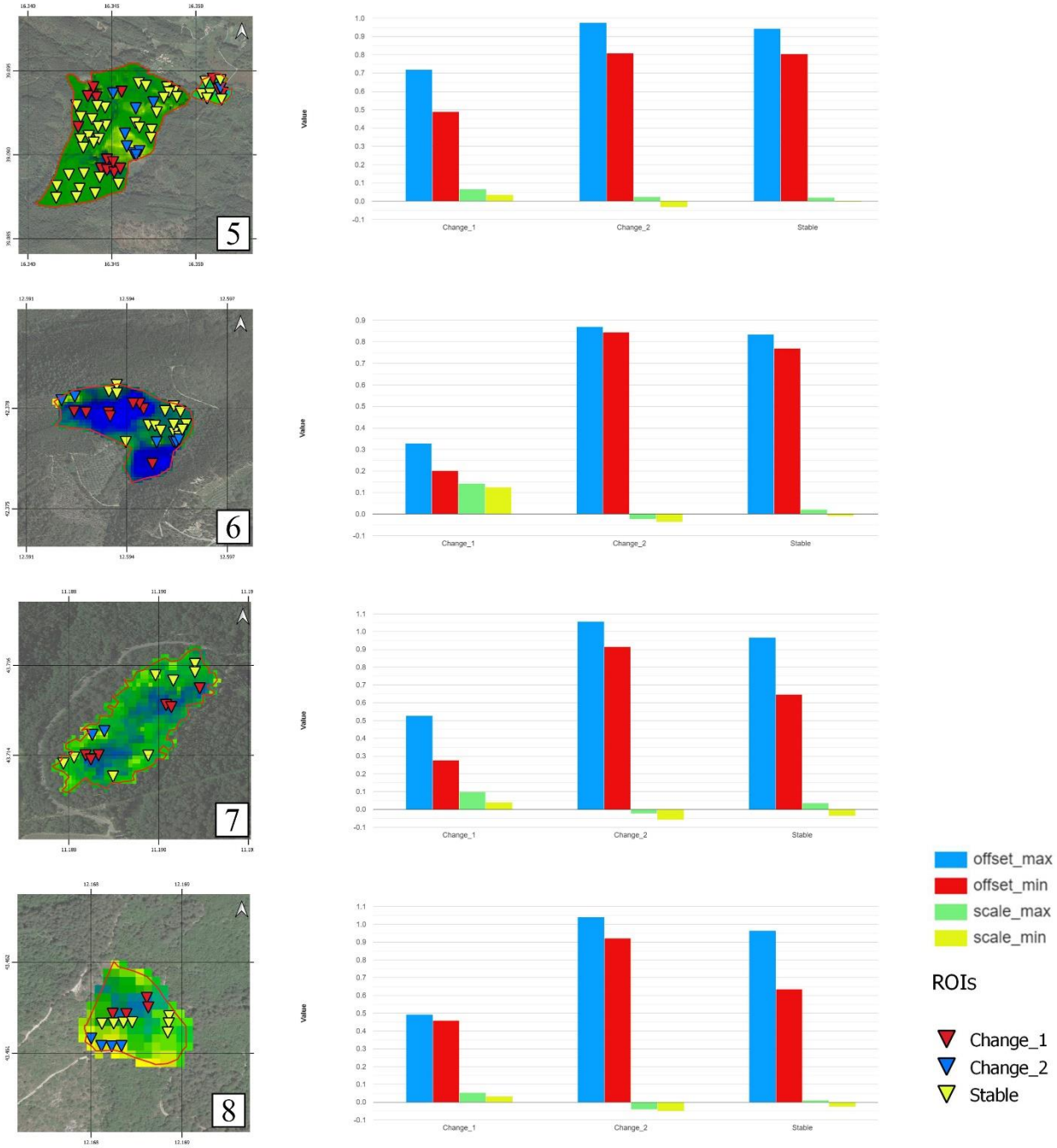

Figure 7. Events 5–8 (referring to IDs in Table 1). Overview image of analyzed cases (RGB: slope, offset, slope) and graph of pixel value in selected ROIs.

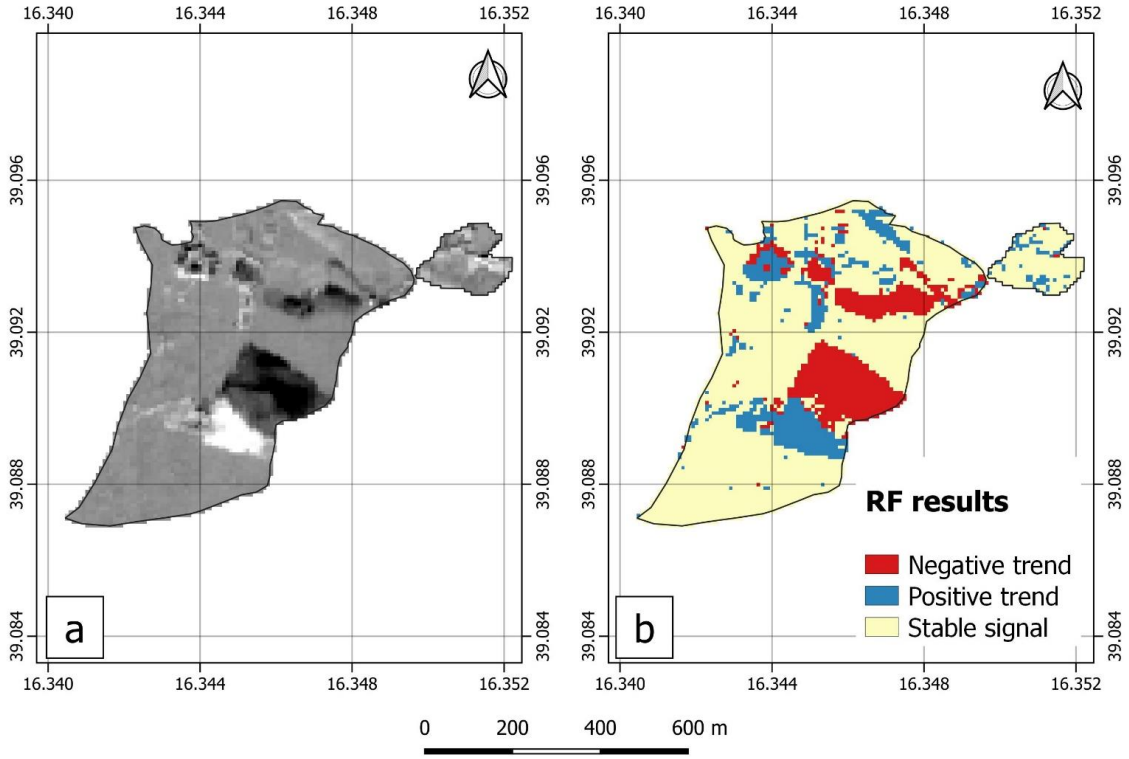

Figure 8. Comparison between (**a**) single-band image of slope (scales): positive values are light, negative values are dark, grey represents values very close to 0; and (**b**) RF results.

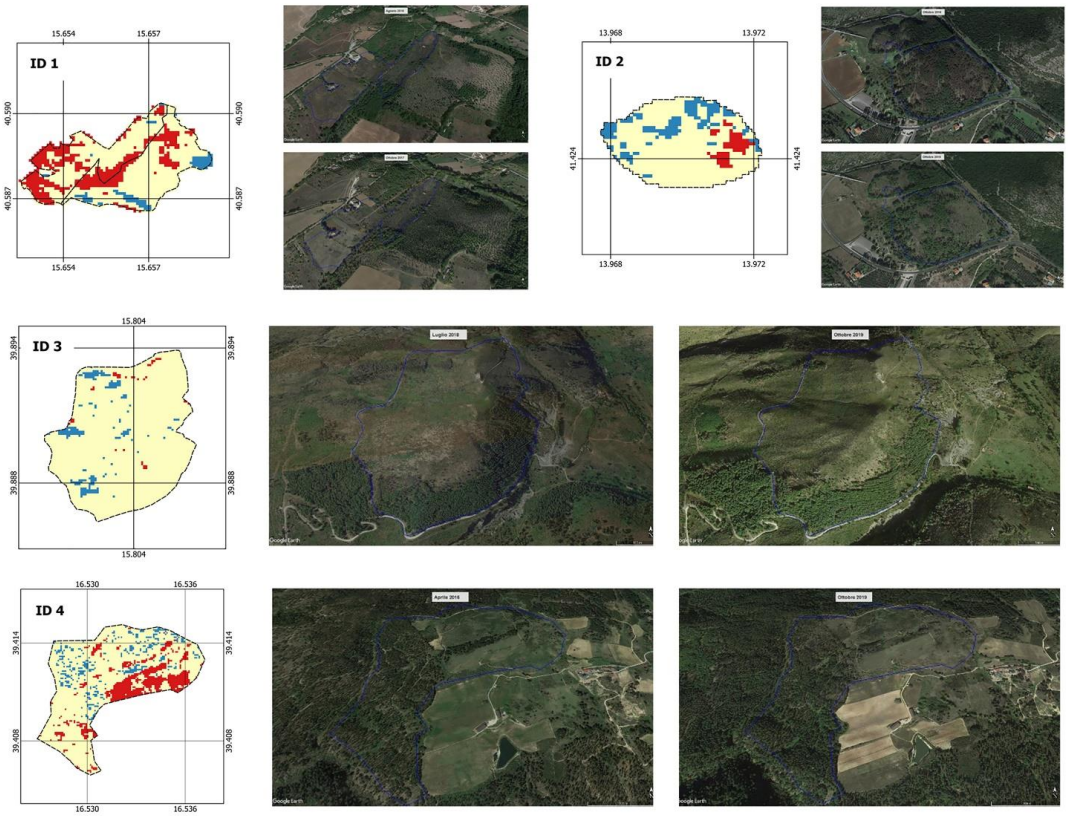

Figure 9. Events 1–4 (referring to IDs in Table 1) and comparison with high-resolution images from Google Earth.

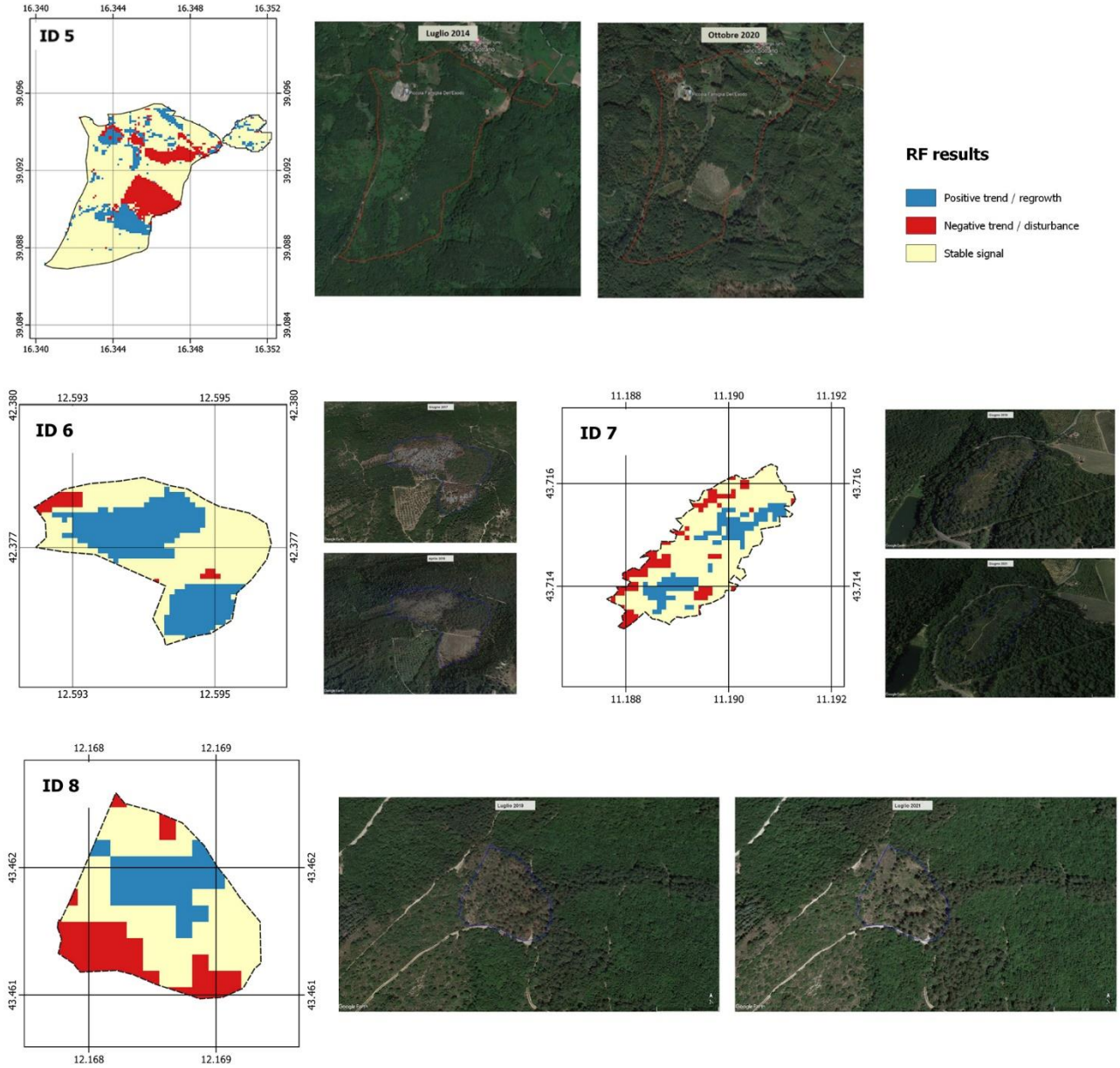

Figure 10. Events 5–8 (referring to IDs in Table 1) and comparison with high-resolution images from Google Earth.

The investigations conducted for this study contributed to assessment of the usefulness of the NDVI time series. The analysis of its temporal and spatial dynamics using LR enabled us to extract useful information and, therefore, transform spectral information into useful vegetation parameters. The analysis of the behavior of the NDVI time signal also enabled us to highlight that 10 m – i.e., the NDVI pixel size – is actually the minimum mapping unit to be considered for satellite Sentinel 2 data.

4. Conclusions

The analysis of changes in land use/land cover has always been a major theme in remote sensing techniques applied to Earth observation. This study has underlined the potential and reliability of the combined use of GEE and Sentinel-2 NDVI time series to identify subtle and small changes in fire-disturbed environs. In fact, the analysis of the temporal behavior of the annual average of NDVI (starting from the year after the fire's occurrence) enabled us to identify, characterize, and categorize even subtle variations

occurring at the Sentinel-2 pixel level (10 m). More broadly, the development of large computing engines and the availability (from cloud platforms) of quite long satellite time series and datasets has recently made it possible to take the use of these techniques to new levels, without the need for prohibitive economic or hardware resources.

In particular, the approach proposed here, based on the use of linear regression (LR) and ML classification, appears to be quite effective and reliable (with an accuracy higher than 0.86) for the identification of changes in LULC in fire-disturbed environs. The calculation was done using hundreds of Sentinel-2L2A multispectral satellite images simultaneously, thanks to the calculation engine and datasets in Google Earth Engine (GEE).

Thanks to the combination of machine learning and the power of Google Earth Engine, it was possible to apply the identification of changes in the LULC to several case studies, in order to obtain a map of the changes that had occurred within the fire-affected areas. The usefulness of such a system is that it can provide, in a fast, rapid, and immediate way, a clearly comprehensible map which can be used to observe the nature of the change and facilitate interventions in the analyzed area. This technique has multiple advantages: (i) ease of use and applicability, and replicability on various temporal and spatial scales; (ii) the fact that it can be easily managed in GEE with an ad-hoc subset, avoiding computational time-out problems; and (iii) the possibility of processing many dozens of events in series. The use of ML/LR applied to maximum NDVI values avoids problems related to seasonal variations or the presence of clouds in the images. At the same time, the use of RF showed more than 75% accuracy in classifying changes from the slope and offset values obtained from LR. In addition, the methodology returned equally reliable results on areas of different sizes, proving to be reapplicable and scalable.

Author Contributions: Conceptualization, R.L., N.A., C.F., and M.D.F.; data curation, R.L., N.A., and C.F.; formal analysis, R.L., N.A., and C.F.; methodology, N.A. and C.F.; project administration, R.L.; software, N.A., C.F., and G.C.; validation, A.A. and G.C.; visualization, A.A., G.C., and M.D.F.; writing—original draft, N.A. and C.F.; writing—review and editing, R.L., N.A., and C.F. All authors have read and agreed to the published version of the manuscript.

Funding: This research received no external funding.

Data Availability Statement: An example of the data used (ID5 in Table 1), as well as the code, used, can be found at: https://code.earthengine.google.com/ed6c76a1b8eb742f825e072e0c2c7264?noload=true.

Acknowledgments: In this section, you can acknowledge any support given which is not covered by the author contribution or funding sections. This may include administrative and technical support, or donations in kind (e.g., materials used for experiments).

Conflicts of Interest: The authors declare no conflict of interest.

References

1. Hermosilla, T.; Wulder, M.A.; White, J.C.; Coops, N.C.; Hobart, G.W. Disturbance-Informed Annual Land Cover Classification Maps of Canada's Forested Ecosystems for a 29-Year Landsat Time Series. *Can. J. Remote Sens.* **2018**, *44*, 67–87. [CrossRef]
2. Wulder, M.A.; Loveland, T.R.; Roy, D.P.; Crawford, C.J.; Masek, J.G.; Woodcock, C.E.; Allen, R.G.; Anderson, M.C.; Belward, A.S.; Cohen, W.B.; et al. Current Status of Landsat Program, Science, and Applications. *Remote Sens. Environ.* **2019**, *225*, 127–147. [CrossRef]
3. Woodcock, C.E.; Allen, R.; Anderson, M.; Belward, A.; Bindschadler, R.; Cohen, W.; Gao, F.; Goward, S.N.; Helder, D.; Helmer, E.; et al. Free Access to Landsat Imagery. *Science* **2008**, *320*, 1011. [CrossRef]
4. Wulder, M.A.; Masek, J.G.; Cohen, W.B.; Loveland, T.R.; Woodcock, C.E. Opening the Archive: How Free Data Has Enabled the Science and Monitoring Promise of Landsat. *Remote Sens. Environ.* **2012**, *122*, 2–10. [CrossRef]
5. Zhu, Z.; Wulder, M.A.; Roy, D.P.; Woodcock, C.E.; Hansen, M.C.; Radeloff, V.C.; Healey, S.P.; Schaaf, C.; Hostert, P.; Strobl, P.; et al. Benefits of the Free and Open Landsat Data Policy. *Remote Sens. Environ.* **2019**, *224*, 382–385. [CrossRef]
6. Wulder, M.A.; White, J.C.; Loveland, T.R.; Woodcock, C.E.; Belward, A.S.; Cohen, W.B.; Fosnight, E.A.; Shaw, J.; Masek, J.G.; Roy, D.P. The Global Landsat Archive: Status, Consolidation, and Direction. *Remote Sens. Environ.* **2016**, *185*, 271–283. [CrossRef]
7. Malenovský, Z.; Rott, H.; Cihlar, J.; Schaepman, M.E.; García-Santos, G.; Fernandes, R.; Berger, M. Sentinels for Science: Potential of Sentinel-1, -2, and -3 Missions for Scientific Observations of Ocean, Cryosphere, and Land. *Remote Sens. Environ.* **2012**, *120*, 91–101. [CrossRef]

8. Belenguer-Plomer, M.A.; Tanase, M.A.; Fernandez-Carrillo, A.; Chuvieco, E. Burned Area Detection and Mapping Using Sentinel-1 Backscatter Coefficient and Thermal Anomalies. *Remote Sens. Environ.* **2019**, *233*, 111345. [CrossRef]
9. Amitrano, D.; Martino, G.D.; Iodice, A.; Mitidieri, F.; Papa, M.N.; Riccio, D.; Ruello, G. Sentinel-1 for Monitoring Reservoirs: A Performance Analysis. *Remote Sens.* **2014**, *6*, 10676–10693. [CrossRef]
10. Caballero, I.; Ruiz, J.; Navarro, G. Sentinel-2 Satellites Provide Near-Real Time Evaluation of Catastrophic Floods in the West Mediterranean. *Water* **2019**, *11*, 2499. [CrossRef]
11. De Luca, G.; Modica, G.; Fattore, C.; Lasaponara, R. Unsupervised Burned Area Mapping in a Protected Natural Site. An Approach Using SAR Sentinel-1 Data and K-Mean Algorithm. In Proceedings of the Computational Science and Its Applications—ICCSA 2020, Cagliari, Italy, 1–4 July 2020; Gervasi, O., Murgante, B., Misra, S., Garau, C., Blečić, I., Taniar, D., Apduhan, B.O., Rocha, A.M.A.C., Tarantino, E., Torre, C.M., et al., Eds.; Springer: Cham, Switzerland, 2020; pp. 63–77.
12. Fletcher, K. *Sentinel 1: ESA's Radar Observatory Mission for GMES Operational Services*; European Space Agency: Paris, France, 2012.
13. Fabre, S.; Elger, A.; Riviere, T. Exploitation of sentinel-2 images for long-term vegetation monitoring at a former ore processing site. *Int. Arch. Photogramm. Remote Sens. Spat. Inf. Sci.* **2020**, *XLIII-B3-2020*, 1533–1537. [CrossRef]
14. Nguyen, T.T.H.; Chau, T.N.Q.; Pham, T.A.; Tran, T.X.P.; Phan, T.H.; Pham, T.M.T. Mapping Land Use/Land Cover Using a Combination of Radar Sentinel-1A and Sentinel-2A Optical Images. *IOP Conf. Ser. Earth Environ. Sci.* **2021**, *652*, 012021. [CrossRef]
15. Bruzzone, L.; Bovolo, F.; Paris, C.; Solano-Correa, Y.T.; Zanetti, M.; Fernandez-Prieto, D. Analysis of Multitemporal Sentinel-2 Images in the Framework of the ESA Scientific Exploitation of Operational Missions. In Proceedings of the 2017 9th International Workshop on the Analysis of Multitemporal Remote Sensing Images (MultiTemp), Brugge, Belgium, 27–29 June 2017; pp. 1–4.
16. Copernicus Open Access Hub. Available online: https://scihub.copernicus.eu/ (accessed on 7 February 2022).
17. Nguyen, N.V.; Trinh, T.H.T.; Pham, H.T.; Tran, T.T.T.; Pham, L.T.; Nguyen, C.T. Land Cover Classification Based on Cloud Computing Platform. *J. Southwest Jiaotong Univ.* **2020**, *55*, 61. [CrossRef]
18. Fattore, C.; Abate, N.; Faridani, F.; Masini, N.; Lasaponara, R. Google Earth Engine as Multi-Sensor Open-Source Tool for Supporting the Preservation of Archaeological Areas: The Case Study of Flood and Fire Mapping in Metaponto, Italy. *Sensors* **2021**, *21*, 1791. [CrossRef]
19. Healey, S.P.; Cohen, W.B.; Yang, Z.; Kenneth Brewer, C.; Brooks, E.B.; Gorelick, N.; Hernandez, A.J.; Huang, C.; Joseph Hughes, M.; Kennedy, R.E.; et al. Mapping Forest Change Using Stacked Generalization: An Ensemble Approach. *Remote Sens. Environ.* **2018**, *204*, 717–728. [CrossRef]
20. Long, T.; Zhang, Z.; He, G.; Jiao, W.; Tang, C.; Wu, B.; Zhang, X.; Wang, G.; Yin, R. 30 m Resolution Global Annual Burned Area Mapping Based on Landsat Images and Google Earth Engine. *Remote Sens.* **2019**, *11*, 489. [CrossRef]
21. Li, W.; Du, Z.; Ling, F.; Zhou, D.; Wang, H.; Gui, Y.; Sun, B.; Zhang, X. A Comparison of Land Surface Water Mapping Using the Normalized Difference Water Index from TM, ETM+ and ALI. *Remote Sens.* **2013**, *5*, 5530–5549. [CrossRef]
22. Guariglia, A.; Buonamassa, A.; Losurdo, A.; Saladino, R.; Trivigno, M.L.; Zaccagnino, A.; Colangelo, A. A Multisource Approach for Coastline Mapping and Identification of Shoreline Changes. *Ann. Geophys.* **2006**, *49*, 295–304. [CrossRef]
23. Pulvirenti, L.; Squicciarino, G.; Fiori, E.; Fiorucci, P.; Ferraris, L.; Negro, D.; Gollini, A.; Severino, M.; Puca, S. An Automatic Processing Chain for Near Real-Time Mapping of Burned Forest Areas Using Sentinel-2 Data. *Remote Sens.* **2020**, *12*, 674. [CrossRef]
24. Schmid, J.N. Using Google Earth Engine for Landsat NDVI Time Series Analysis to Indicate the Present Status of Forest Stands. Bachelor's Thesis, Georg-August-Universität Göttingen, Göttingen, Germany, 2017. [CrossRef]
25. Xiong, J.; Thenkabail, P.S.; Gumma, M.K.; Teluguntla, P.; Poehnelt, J.; Congalton, R.G.; Yadav, K.; Thau, D. Automated Cropland Mapping of Continental Africa Using Google Earth Engine Cloud Computing. *ISPRS J. Photogramm. Remote Sens.* **2017**, *126*, 225–244. [CrossRef]
26. Vanama, V.S.K.; Mandal, D.; Rao, Y.S. GEE4FLOOD: Rapid Mapping of Flood Areas Using Temporal Sentinel-1 SAR Images with Google Earth Engine Cloud Platform. *J. Appl. Remote Sens.* **2020**, *14*, 034505. [CrossRef]
27. Parente, L.; Mesquita, V.; Miziara, F.; Baumann, L.; Ferreira, L. Assessing the Pasturelands and Livestock Dynamics in Brazil, from 1985 to 2017: A Novel Approach Based on High Spatial Resolution Imagery and Google Earth Engine Cloud Computing. *Remote Sens. Environ.* **2019**, *232*, 111301. [CrossRef]
28. Tamiminia, H.; Salehi, B.; Mahdianpari, M.; Quackenbush, L.; Adeli, S.; Brisco, B. Google Earth Engine for Geo-Big Data Applications: A Meta-Analysis and Systematic Review. *ISPRS J. Photogramm. Remote Sens.* **2020**, *164*, 152–170. [CrossRef]
29. Tsai, Y.H.; Stow, D.; Chen, H.L.; Lewison, R.; An, L.; Shi, L. Mapping Vegetation and Land Use Types in Fanjingshan National Nature Reserve Using Google Earth Engine. *Remote Sens.* **2018**, *10*, 927. [CrossRef]
30. Khelifi, L.; Mignotte, M. Deep Learning for Change Detection in Remote Sensing Images: Comprehensive Review and Meta-Analysis. *arXiv* **2020**, arXiv200605612. [CrossRef]
31. Jaturapitpornchai, R.; Matsuoka, M.; Kanemoto, N.; Kuzuoka, S.; Ito, R.; Nakamura, R. Newly Built Construction Detection in SAR Images Using Deep Learning. *Remote Sens.* **2019**, *11*, 1444. [CrossRef]
32. Yang, M.; Jiao, L.; Liu, F.; Hou, B.; Yang, S. Transferred Deep Learning-Based Change Detection in Remote Sensing Images. *IEEE Trans. Geosci. Remote Sens.* **2019**, *57*, 6960–6973. [CrossRef]
33. Lyu, H.; Lu, H.; Mou, L. Learning a Transferable Change Rule from a Recurrent Neural Network for Land Cover Change Detection. *Remote Sens.* **2016**, *8*, 506. [CrossRef]

34. Vaglio Laurin, G.; Francini, S.; Luti, T.; Chirici, G.; Pirotti, F.; Papale, D. Satellite Open Data to Monitor Forest Damage Caused by Extreme Climate-Induced Events: A Case Study of the Vaia Storm in Northern Italy. *For. Int. J. For. Res.* **2021**, *94*, 407–416. [CrossRef]
35. Kislov, D.E.; Korznikov, K.A.; Altman, J.; Vozmishcheva, A.S.; Krestov, P.V. Extending Deep Learning Approaches for Forest Disturbance Segmentation on Very High-resolution Satellite Images. *Remote Sens. Ecol. Conserv.* **2021**, *7*, 355–368. [CrossRef]
36. Milodowski, D.T.; Mitchard, E.T.A.; Williams, M. Forest Loss Maps from Regional Satellite Monitoring Systematically Underestimate Deforestation in Two Rapidly Changing Parts of the Amazon. *Environ. Res. Lett.* **2017**, *12*, 094003. [CrossRef]
37. Saheed, S.O.; Igbokwe, J.I.; Ojiako, J.C. Comparative Analysis of Change Detection Techniques In Landuse / Landcover Mapping of Oyo Town, Oyo State, Nigeria. *Int. J. Sci. Res. Sci. Technol.* **2020**, 44–62. [CrossRef]
38. Hu, Y.; Dong, Y.; Batunacun. An Automatic Approach for Land-Change Detection and Land Updates Based on Integrated NDVI Timing Analysis and the CVAPS Method with GEE Support. *ISPRS J. Photogramm. Remote Sens.* **2018**, *146*, 347–359. [CrossRef]
39. Jianguang, L.; Danfeng, S.; Feng, H.; Weiwei, Z.; Xiaoke, G. Land Use/Cover Classification with Classification and Regression Tree Applied to MODIS Imagery. *J. Appl. Sci.* **2013**, *13*, 3770–3773.
40. Liu, H.; Zhou, Q. Accuracy Analysis of Remote Sensing Change Detection by Rule-Based Rationality Evaluation with Post-Classification Comparison. *Int. J. Remote Sens.* **2004**, *25*, 1037–1050. [CrossRef]
41. Hughes, M.; Kaylor, S.; Hayes, D. Patch-Based Forest Change Detection from Landsat Time Series. *Forests* **2017**, *8*, 166. [CrossRef]
42. Huang, C.; Goward, S.N.; Masek, J.G.; Thomas, N.; Zhu, Z.; Vogelmann, J.E. An Automated Approach for Reconstructing Recent Forest Disturbance History Using Dense Landsat Time Series Stacks. *Remote Sens. Environ.* **2010**, *114*, 183–198. [CrossRef]
43. Tao, X.; Huang, C.; Zhao, F.; Schleeweis, K.; Masek, J.; Liang, S. Mapping Forest Disturbance Intensity in North and South Carolina Using Annual Landsat Observations and Field Inventory Data. *Remote Sens. Environ.* **2019**, *221*, 351–362. [CrossRef]
44. Chirici, G.; Giannetti, F.; Mazza, E.; Francini, S.; Travaglini, D.; Pegna, R.; White, J.C. Monitoring Clearcutting and Subsequent Rapid Recovery in Mediterranean Coppice Forests with Landsat Time Series. *Ann. For. Sci.* **2020**, *77*, 40. [CrossRef]
45. Kennedy, R.E.; Yang, Z.; Cohen, W.B. Detecting Trends in Forest Disturbance and Recovery Using Yearly Landsat Time Series: 1. LandTrendr—Temporal Segmentation Algorithms. *Remote Sens. Environ.* **2010**, *114*, 2897–2910. [CrossRef]
46. Cohen, W.B.; Yang, Z.; Kennedy, R. Detecting Trends in Forest Disturbance and Recovery Using Yearly Landsat Time Series: 2. TimeSync—Tools for Calibration and Validation. *Remote Sens. Environ.* **2010**, *114*, 2911–2924. [CrossRef]
47. Kennedy, R.; Yang, Z.; Gorelick, N.; Braaten, J.; Cavalcante, L.; Cohen, W.; Healey, S. Implementation of the LandTrendr Algorithm on Google Earth Engine. *Remote Sens.* **2018**, *10*, 691. [CrossRef]
48. Mugiraneza, T.; Nascetti, A.; Ban, Y. Continuous Monitoring of Urban Land Cover Change Trajectories with Landsat Time Series and LandTrendr-Google Earth Engine Cloud Computing. *Remote Sens.* **2020**, *12*, 2883. [CrossRef]
49. Grabska, E.; Hawryło, P.; Socha, J. Continuous Detection of Small-Scale Changes in Scots Pine Dominated Stands Using Dense Sentinel-2 Time Series. *Remote Sens.* **2020**, *12*, 1298. [CrossRef]
50. Zhu, Z.; Woodcock, C.E. Continuous Change Detection and Classification of Land Cover Using All Available Landsat Data. *Remote Sens. Environ.* **2014**, *144*, 152–171. [CrossRef]
51. Arévalo, P.; Bullock, E.L.; Woodcock, C.E.; Olofsson, P. A Suite of Tools for Continuous Land Change Monitoring in Google Earth Engine. *Front. Clim.* **2020**, *2*, 576740. [CrossRef]
52. Jahanifar, K.; Amirnejad, H.; Mojaverian, M.; Azadi, H. Land Change Detection and Effective Factors on Forest Land Use Changes: Application of Land Change Modeler and Multiple Linear Regression. *J. Appl. Sci. Environ. Manag.* **2018**, *22*, 1269. [CrossRef]
53. Morisette, J.T.; Khorram, S.; Mace, T. Land-Cover Change Detection Enhanced with Generalized Linear Models. *Int. J. Remote Sens.* **1999**, *20*, 2703–2721. [CrossRef]
54. Millington, J.D.A.; Perry, G.L.W.; Romero-Calcerrada, R. Regression Techniques for Examining Land Use/Cover Change: A Case Study of a Mediterranean Landscape. *Ecosystems* **2007**, *10*, 562–578. [CrossRef]
55. Khwarahm, N.R.; Qader, S.; Ararat, K.; Fadhil Al-Quraishi, A.M. Predicting and Mapping Land Cover/Land Use Changes in Erbil /Iraq Using CA-Markov Synergy Model. *Earth Sci. Inform.* **2021**, *14*, 393–406. [CrossRef]
56. Ye, J.; Hu, Y.; Zhen, L.; Wang, H.; Zhang, Y. Analysis on Land-Use Change and Its Driving Mechanism in Xilingol, China, during 2000–2020 Using the Google Earth Engine. *Remote Sens.* **2021**, *13*, 5134. [CrossRef]
57. Kennedy, R.E.; Yang, Z.; Cohen, W.B.; Pfaff, E.; Braaten, J.; Nelson, P. Spatial and Temporal Patterns of Forest Disturbance and Regrowth within the Area of the Northwest Forest Plan. *Remote Sens. Environ.* **2012**, *122*, 117–133. [CrossRef]
58. Cohen, W.B.; Yang, Z.; Healey, S.P.; Kennedy, R.E.; Gorelick, N. A LandTrendr Multispectral Ensemble for Forest Disturbance Detection. *Remote Sens. Environ.* **2018**, *205*, 131–140. [CrossRef]
59. Schneibel, A.; Stellmes, M.; Röder, A.; Frantz, D.; Kowalski, B.; Haß, E.; Hill, J. Assessment of Spatio-Temporal Changes of Smallholder Cultivation Patterns in the Angolan Miombo Belt Using Segmentation of Landsat Time Series. *Remote Sens. Environ.* **2017**, *195*, 118–129. [CrossRef]
60. Kennedy, R.E.; Yang, Z.; Braaten, J.; Copass, C.; Antonova, N.; Jordan, C.; Nelson, P. Attribution of Disturbance Change Agent from Landsat Time-Series in Support of Habitat Monitoring in the Puget Sound Region, USA. *Remote Sens. Environ.* **2015**, *166*, 271–285. [CrossRef]
61. Canty, M.J.; Nielsen, A.A.; Conradsen, K.; Skriver, H. Statistical Analysis of Changes in Sentinel-1 Time Series on the Google Earth Engine. *Remote Sens.* **2020**, *12*, 46. [CrossRef]

62. Hamunyela, E.; Rosca, S.; Mirt, A.; Engle, E.; Herold, M.; Gieseke, F.; Verbesselt, J. Implementation of BFASTmonitor Algorithm on Google Earth Engine to Support Large-Area and Sub-Annual Change Monitoring Using Earth Observation Data. *Remote Sens.* **2020**, *12*, 2953. [CrossRef]
63. Colin, B.; Mengersen, K. Estimating Spatial and Temporal Trends in Environmental Indices Based on Satellite Data: A Two-Step Approach. *Sensors* **2019**, *19*, 361. [CrossRef]
64. Gorelick, N. *Google Earth Engine*; American Geophysical Union: Vienna, Austria, 2013; p. 11997.
65. Gorelick, N.; Hancher, M.; Dixon, M.; Ilyushchenko, S.; Thau, D.; Moore, R. Google Earth Engine: Planetary-Scale Geospatial Analysis for Everyone. *Remote Sens. Environ.* **2017**, *202*, 18–27. [CrossRef]
66. Kumar, S.; Arya, S. Change Detection Techniques for Land Cover Change Analysis Using Spatial Datasets: A Review. *Remote Sens. Earth Syst. Sci.* **2021**, *4*, 172–185. [CrossRef]
67. Kumar, L.; Mutanga, O. Google Earth Engine Applications Since Inception: Usage, Trends, and Potential. *Remote Sens.* **2018**, *10*, 1509. [CrossRef]
68. Wang, L.; Diao, C.; Xian, G.; Yin, D.; Lu, Y.; Zou, S.; Erickson, T.A. A Summary of the Special Issue on Remote Sensing of Land Change Science with Google Earth Engine. *Remote Sens. Environ.* **2020**, *248*, 112002. [CrossRef]
69. Mahdianpari, M.; Salehi, B.; Mohammadimanesh, F.; Homayouni, S.; Gill, E. The First Wetland Inventory Map of Newfoundland at a Spatial Resolution of 10 m Using Sentinel-1 and Sentinel-2 Data on the Google Earth Engine Cloud Computing Platform. *Remote Sens.* **2019**, *11*, 43. [CrossRef]
70. Mutanga, O.; Kumar, L. Google Earth Engine Applications. *Remote Sens.* **2019**, *11*, 591. [CrossRef]
71. Campos-Taberner, M.; Moreno-Martínez, Á.; García-Haro, F.J.; Camps-Valls, G.; Robinson, N.P.; Kattge, J.; Running, S.W. Global Estimation of Biophysical Variables from Google Earth Engine Platform. *Remote Sens.* **2018**, *10*, 1167. [CrossRef]
72. Deines, J.M.; Kendall, A.D.; Crowley, M.A.; Rapp, J.; Cardille, J.A.; Hyndman, D.W. Mapping Three Decades of Annual Irrigation across the US High Plains Aquifer Using Landsat and Google Earth Engine. *Remote Sens. Environ.* **2019**, *233*, 111400. [CrossRef]
73. DeVries, B.; Huang, C.; Armston, J.; Huang, W.; Jones, J.W.; Lang, M.W. Rapid and Robust Monitoring of Flood Events Using Sentinel-1 and Landsat Data on the Google Earth Engine. *Remote Sens. Environ.* **2020**, *240*, 111664. [CrossRef]
74. Horowitz, F. MODIS Daily Land Surface Temperature Estimates in Google Earth Engine as an Aid in Geothermal Energy Siting. In Proceedings of the World Geothermal Congress, Melbourne, Australia, 19–25 April 2015.
75. Bey, A.; Jetimane, J.; Lisboa, S.N.; Ribeiro, N.; Sitoe, A.; Meyfroidt, P. Mapping Smallholder and Large-Scale Cropland Dynamics with a Flexible Classification System and Pixel-Based Composites in an Emerging Frontier of Mozambique. *Remote Sens. Environ.* **2020**, *239*, 111611. [CrossRef]
76. Lemoine, G.; Leo, O. Crop Mapping Applications at Scale: Using Google Earth Engine to Enable Global Crop Area and Status Monitoring Using Free and Open Data Sources. In Proceedings of the 2015 IEEE International Geoscience and Remote Sensing Symposium (IGARSS), Milan, Italy, 26–31 July 2015; pp. 1496–1499.
77. Sazib, N.; Mladenova, I.; Bolten, J. Leveraging the Google Earth Engine for Drought Assessment Using Global Soil Moisture Data. *Remote Sens.* **2018**, *10*, 1265. [CrossRef]
78. Sidhu, N.; Pebesma, E.; Câmara, G. Using Google Earth Engine to Detect Land Cover Change: Singapore as a Use Case. *Eur. J. Remote Sens.* **2018**, *51*, 486–500. [CrossRef]
79. Orengo, H.A.; Conesa, F.C.; Garcia-Molsosa, A.; Lobo, A.; Green, A.S.; Madella, M.; Petrie, C.A. Automated Detection of Archaeological Mounds Using Machine-Learning Classification of Multisensor and Multitemporal Satellite Data. *Proc. Natl. Acad. Sci. USA* **2020**, *117*, 18240–18250. [CrossRef] [PubMed]
80. Hansen, M.C.; Potapov, P.V.; Moore, R.; Hancher, M.; Turubanova, S.A.; Tyukavina, A.; Thau, D.; Stehman, S.V.; Goetz, S.J.; Loveland, T.R.; et al. High-Resolution Global Maps of 21st-Century Forest Cover Change. *Science* **2013**, *342*, 850–853. [PubMed]
81. Hansen, C.H. *Google Earth Engine as a Platform for Making Remote Sensing of Water Resources a Reality for Monitoring Inland Waters*; Department of Civil and Environmental Engineering: Suite, UT, USA, 2015. [CrossRef]
82. Lasaponara, R.; Abate, N.; Masini, N. On the Use of Google Earth Engine and Sentinel Data to Detect "Lost" Sections of Ancient Roads. The Case of Via Appia. *IEEE Geosci. Remote Sens. Lett.* **2021**, *19*. [CrossRef]
83. Pekel, J.-F.; Cottam, A.; Gorelick, N.; Belward, A.S. High-Resolution Mapping of Global Surface Water and Its Long-Term Changes. *Nature* **2016**, *540*, 418–422. [CrossRef]
84. Pepe, M.; Parente, C. Recognition of Burned Area Change of Detection Analysis Using Images Derived from Satellite Sentinel-2: Case Studio of Sorrento Penisola, Italy. *J. Appl. Eng. Sci.* **2018**, *16*, 225–232. [CrossRef]
85. Khairani, N.A.; Sutoyo, E. Application of K-Means Clustering Algorithm for Determination of Fire-Prone Areas Utilizing Hotspots in West Kalimantan Province. *Int. J. Adv. Data Inf. Syst.* **2020**, *1*, 9–16. [CrossRef]
86. Candra, D.S.; Phinn, S.; Scarth, P. Cloud and Cloud Shadow Masking for Sentinel-2 Using Multitemporal Images in Global Area. *Int. J. Remote Sens.* **2020**, *41*, 2877–2904. [CrossRef]
87. Telesca, L.; Lasaponara, R. Analysis of Time-Scaling Properties in Forest-Fire Sequence Observed in Italy. *Ecol. Model.* **2010**, *221*, 90–93. [CrossRef]
88. Telesca, L. Time-Clustering of Natural Hazards. *Nat. Hazards* **2007**, *40*, 593–601. [CrossRef]
89. Telesca, L.; Lasaponara, R. Discriminating Dynamical Patterns in Burned and Unburned Vegetational Covers by Using SPOT-VGT NDVI Data. *Geophys. Res. Lett.* **2005**, *32*, L21401. [CrossRef]

90. Lanorte, A.; Lasaponara, R.; Lovallo, M.; Telesca, L. Fisher–Shannon Information Plane Analysis of SPOT/VEGETATION Normalized Difference Vegetation Index (NDVI) Time Series to Characterize Vegetation Recovery after Fire Disturbance. *Int. J. Appl. Earth Obs. Geoinf.* **2014**, *26*, 441–446. [CrossRef]
91. Telesca, L.; Lasaponara, R. Quantifying Intra-Annual Persistent Behaviour in SPOT-VEGETATION NDVI Data for Mediterranean Ecosystems of Southern Italy. *Remote Sens. Environ.* **2006**, *101*, 95–103. [CrossRef]
92. Jiang, Z.; Huete, A.R. Linearization of NDVI Based on Its Relationship with Vegetation Fraction. *Photogramm. Eng. Remote Sens.* **2010**, *76*, 965–975. [CrossRef]
93. Rouse, J.; Haas, R.H.; Deering, D.; Schell, J.A.; Harlan, J. *Monitoring the Vernal Advancement and Retrogradation (Green Wave Effect) of Natural Vegetation*; BSC 5-21857; Texas A&M University: College Station, TX, USA, 1974.
94. Justice, C.O.; Townshend, J.R.G.; Holben, B.N.; Tucker, C.J. Analysis of the Phenology of Global Vegetation Using Meteorological Satellite Data. *Int. J. Remote Sens.* **1985**, *6*, 1271–1318. [CrossRef]
95. Mbatha, N.; Xulu, S. Time Series Analysis of MODIS-Derived NDVI for the Hluhluwe-Imfolozi Park, South Africa: Impact of Recent Intense Drought. *Climate* **2018**, *6*, 95. [CrossRef]
96. Forkel, M.; Carvalhais, N.; Verbesselt, J.; Mahecha, M.D.; Neigh, C.S.R.; Reichstein, M. Trend Change Detection in NDVI Time Series: Effects of Inter-Annual Variability and Methodology. *Remote Sens.* **2013**, *5*, 2113–2144. [CrossRef]
97. Buchhorn, M.; Smets, B.; Bertels, L.; Lesiv, M.; Tsendbazar, N.-E.; Herold, M.; Fritz, S. Copernicus Global Land Service: Land Cover 100m: Collection 2: Epoch 2015: Globe 2019. Available online: https://land.copernicus.eu/global/products/lc (accessed on 3 August 2022).
98. Buchhorn, M.; Lesiv, M.; Tsendbazar, N.-E.; Herold, M.; Bertels, L.; Smets, B. Copernicus Global Land Cover Layers—Collection 2. *Remote Sens.* **2020**, *12*, 1044. [CrossRef]
99. Copernicus Land Monitoring Service—Corine Land Cover—European Environment Agency. Available online: https://www.eea.europa.eu/data-and-maps/data/copernicus-land-monitoring-service-corine (accessed on 7 February 2022).
100. Farr, T.G.; Rosen, P.A.; Caro, E.; Crippen, R.; Duren, R.; Hensley, S.; Kobrick, M.; Paller, M.; Rodriguez, E.; Roth, L.; et al. The Shuttle Radar Topography Mission. *Rev. Geophys.* **2007**, *45*. [CrossRef]
101. Tarquini, S.; Isola, I.; Favalli, M.; Mazzarini, F.; Bisson, M.; Pareschi, M.T.; Boschi, E. TINITALY/01: A New Triangular Irregular Network of Italy. *Ann. Geophys.* **2009**, *50*. [CrossRef]
102. Tarquini, S.; Isola, I.; Favalli, M.; Battistini, A. TINITALY, a Digital Elevation Model of Italy with a 10 Meters Cell Size 2007, about 3000 M grid cells, about 17 Gb of disk memory. Available online: https://tinitaly.pi.ingv.it/ (accessed on 3 August 2022).
103. Tarrio, K.; Tang, X.; Masek, J.G.; Claverie, M.; Ju, J.; Qiu, S.; Zhu, Z.; Woodcock, C.E. Comparison of Cloud Detection Algorithms for Sentinel-2 Imagery. *Sci. Remote Sens.* **2020**, *2*, 100010. [CrossRef]
104. Ujaval, G. End-to-End Google Earth Engine Course. Spatial Thoughts. Available online: https://courses.spatialthoughts.com/end-to-end-gee.html (accessed on 3 August 2022).
105. Shumway, R.H.; Stoffer, D.S. *Time Series Analysis and Its Applications: With R Examples*, 4th ed.; Springer Texts in Statistics; Springer International Publishing: Berlin/Heidelberg, Germany, 2017; ISBN 978-3-319-52451-1.
106. Wessels, K.J.; Van den Bergh, F.; Roy, D.P.; Salmon, B.P.; Steenkamp, K.C.; MacAlister, B.; Swanepoel, D.; Jewitt, D. Rapid Land Cover Map Updates Using Change Detection and Robust Random Forest Classifiers. *Remote Sens.* **2016**, *8*, 888. [CrossRef]
107. Amini, S.; Saber, M.; Rabiei-Dastjerdi, H.; Homayouni, S. Urban Land Use and Land Cover Change Analysis Using Random Forest Classification of Landsat Time Series. *Remote Sens.* **2022**, *14*, 2654. [CrossRef]
108. Breiman, L. Random Forests. *Mach. Learn.* **2001**, *45*, 5–32. [CrossRef]
109. Millard, K.; Richardson, M. On the Importance of Training Data Sample Selection in Random Forest Image Classification: A Case Study in Peatland Ecosystem Mapping. *Remote Sens.* **2015**, *7*, 8489–8515. [CrossRef]